Biomass and Bioenergy 143 (2020) 105843

Contents lists available at ScienceDirect

Biomass and Bioenergy

journal homepage: http://www.elsevier.com/locate/biombioe

Investigations of molybdenum-promoted manganese-based solid sorbents for H_2S capture

Jianyu Ma [a], Kumar R. Rout [b], Maximilian Sauer [a,1], Mehdi Mahmoodinia [a], Edd A. Blekkan [a,*]

[a] Dept. of Chemical Engineering, Norwegian University of Science and Technology (NTNU), NO-7491, Trondheim, Norway
[b] SINTEF Industry, NO-7465, Trondheim, Norway

ARTICLE INFO

Keywords:
Gas cleaning
HTSS
Manganese oxide
Molybdenum promoter

ABSTRACT

The promotion effect of Mo-addition to alumina-supported Mn-based sorbents for high-temperature desulphurization was explored. A series of Mn-based sorbents with fixed Mn-loading and different Mo-loadings were prepared by the wet impregnation method and both fresh and used sorbents were characterized with respect to their physical and chemical properties. The sorbents were active for H_2S removal at 600 °C and could be regenerated by oxidation in diluted air. The sorbents were subjected to 10 repeated sorption/regeneration cycles, and some loss of capacity occurred during the cycles. The results show that Mo-addition promotes the Mn-based sulfur sorbent performance both in terms of capacity and stability. Over the range investigated (0–8 wt% Mo added to a 15 wt% Mn sorbent), the improvement increased with an increasing amount of Mo added. The sample with the highest Mo-addition (15Mn8Mo) also retained the capacity best, as over 90% of the capacity remained after 10 sorption-regeneration cycles, in spite of suffering the most from sintering (observed as loss in surface area, increased pore size, and growth in Mn particle size). Characterization of the fresh and used samples using XRD and Raman spectroscopy indicates that a mixed Mn–Mo oxide suggested to be MnMoO4 plays a role in the promotion mechanism. The sorbent, 15Mn8Mo, is suggested to be promising for high-temperature desulphurization of bio-syngas.

1. Introduction

Biomass gasification and subsequent fuel synthesis is a realistic route to 2nd generation biofuels, which are considered as one of the key alternatives to fossil fuels and as such can contribute to a solution to the energy crisis [1]. However, the produced syngas contains undesired species and contaminants that have severe detrimental effects on downstream equipment and catalysts [2]. The raw syngas produced in the gasifier contains particulate species, tar, sulfur compounds, nitrogen compounds, etc., the types and amounts of which depend strongly on the feedstock, gasification process and conditions [3,4]. Therefore, gas cleaning and gas conditioning are important steps, and high-temperature gas cleaning is considered to be beneficial in terms of energy efficiency and investment from a process design point of view [5]. A key contaminant in biomass-derived syngas is sulfur, present mainly as hydrogen sulfide and COS. Sulfur compounds can lead to severe corrosion of equipment, rapid deactivation of catalysts and environmental pollution [6,7]. Xiangmei Meng and colleagues summarized the typically allowable sulfur levels for various syngas applications [7]. For example, the catalysts applied for methanol synthesis or Fischer-Tropsch synthesis are very sensitive to the sulfur content and require concentrations below 1 ppmv H_2S in the feed gas [8–10]. Hence, complete sulfur capture from bio-syngas is necessary for its use as a feedstock for further catalytic conversion.

Conventionally, sulfur compounds are removed chemically or physically by solvent-based methods, classified as low-temperature sulfur removal methods [11]. Importantly, independently of which solvents are utilized, the cleaning step is costly in terms of investments and reduces the energy efficiency of the overall process due to the need for cooling, normally from 800 to 900 °C to lower than 100 °C [11], and subsequent reheating of the gas. High-temperature desulphurization with metal oxide based solid sorbents is thus of interest since this route can potentially reduce the investment and also reduce the energy loss [5].

Westmoreland and Harrison [12] proposed eleven candidate solid sorbents based on the transition metals zinc, iron, manganese,

* Corresponding author.
E-mail address: edd.a.blekkan@ntnu.no (E.A. Blekkan).
[1] Present Address: Technical University of Munich, Germany.

https://doi.org/10.1016/j.biombioe.2020.105843
Received 31 December 2019; Received in revised form 9 October 2020; Accepted 19 October 2020
Available online 6 November 2020

molybdenum, vanadium, calcium, strontium, barium, cobalt, copper, and tungsten, which all show the thermodynamic feasibility for high-temperature desulphurization. Reactions involved in high-temperature desulphurization with solid sorbents are listed in Equations (1)-(5) below [7]:

$$M_xO_y(s) + xH_2S(g) + (y-x)H_2(g) \rightarrow xMS(s) + yH_2O(g) \quad (1)$$

$$MS(s) + H_2O(g) \rightarrow MO(s) + H_2S(g) \quad (2)$$

$$xMS(s) + \left(\frac{y}{2}\right)SO_2(g) \rightarrow M_xO_y + \left(x+\frac{y}{2}\right)S(g) \quad (3)$$

$$xMS(s) + \left(\frac{y}{2}\right)O_2(g) \rightarrow M_xO_y(s) + xSO_2(g) \quad (4)$$

$$MS(s) + 2O_2(g) \rightarrow MnSO_4(s) \quad (5)$$

where M represents metals. H_2S can be removed from the gas phase by metal oxides through reaction 1. The produced metal sulfide can then be regenerated back to metal oxide through reactions 2–4, with various types of sulfur species formation. All reactions can occur under medium to high temperature, i.e. 400–900 °C, replacing conventional scrubber technology [6]. Regenerative sorbents can be adapted to a chemical looping process, thus reducing the consumption of sorbents and the size of the apparatus, and the sulfur can be recovered and used in other applications, such as the Claus process [6].

Among all proposed sorbents Ca– Zn-, Cu-, Fe- and Mn-based materials are often studied as potential candidates [6,7]. However, the high temperatures (>400 °C) can induce carbide formation for Fe-based sorbents, and facilitate the reduction to the metallic state for Zn- and Cu-based sorbents [6,7]. These factors suppress the sorbent capacity and may lead to unexpected process problems. Ca-based sorbents are normally applied as an additive to fluid bed gasifiers as in-situ desulphurization sorbents. Reaction 1 leads to calcium sulfide which is unstable and highly reactive with O_2, forming stable calcium sulfate through Reaction 5, making regeneration difficult [7]. Mn-based solid sorbents, in contrast, have a promising performance at high temperatures, due to their high thermal stability, resistance to reduction and volatilization [7,13]. For example, metallic Mn cannot be formed below 1200 °C, hence the volatilization of metal that can be observed for Cu and Zn does not occur for Mn. In addition, Mn-based solid sorbents have better sorption kinetics for the desulphurization process [6,7,13].

An important aspect when selecting a sorbent is its durability and stability under reaction conditions. Support materials play an important role in this respect by determining the strength of metal-oxide/support interactions. The role of support materials in sorbent performance has been investigated recently in our group [14], and a series of sorbent materials consisting of manganese oxide supported on various carriers; Al_2O_3, TiO_2, ZrO_2 and CeO_2, have been investigated for the desulphurization process. The results showed noticeable differences in the capacity and stability of the sorbents supported on different materials. The variations in sorbent properties have been discussed based on the metal-oxide/support interactions, as other variables during the sample preparations and testing were considered to be the same. Although the sorbent supported on ZrO_2 showed the best stability, the sorbent with Al_2O_3 support showed higher overall capacities combined with acceptable stability. Hence, Al_2O_3 is selected as support for sorbent preparation based on a comprehensive consideration of stability and capacity.

Another approach to improve the sorbent performance is by the addition of other elements, typically metals, as promoters. Copper, zinc, and iron have been studied as promoters to improve the performance of Mn-based sorbents [15–17], however, these metals suffer from problems already mentioned. Westmoreland and Harrison reported Mo as a potential candidate for a desulphurization sorbent. Zhang et al. [18] also found that the addition of Mo can promote the desulphurization capacity of Mn-based sorbents. Wang et al. [19] reported that Mo can increase the desulphurization efficiency of Fe-based sorbents. Hong et al. [20] studied the effects of Mo addition on Mn–Fe-based solid sorbents and confirmed that Mo can substantially improve the stability of these sorbents. The improved performance of Mn-based solid sorbents was linked to the formation of manganese (II) molybdate (Mn(MoO4)), which in principle is a combination of the most stable Mn and Mo oxides under the reducing syngas environment, MnO and MoO3, respectively. This binary metal oxide is widely used for catalysts, batteries and wastewater treatment adsorbents [21–23].

Testing sorbents is a challenging task. Bakker et al. proposed five requirements for desulphurization sorbents screening [24]:

(1) High equilibrium constant and fast kinetics for the sulfidation reaction;
(2) High selectivity towards sulfur capture to minimize side reactions;
(3) Resistance to reduction by H_2 in order to preserve the fuel or chemical value of the biomass gas;
(4) High mechanical stability to minimize mass losses by attrition.
(5) Good regeneration capabilities at an optimal cost.

Based on the literature review, and including the recent studies in our group [25,26], manganese is selected as the main active component for the sorbent used for sulfur removal in this study. In a previous paper we investigated two loadings, 15 wt% and 30 wt%, and found that the lower loading gave sorbents with the best stability through repeated sorption-regeneration cycles [25]. Hence, 15 wt% is selected as the loading for Mn in this work. γ-Alumina is much used as a support for many applications and is selected as the support material in this work due to the relatively good stability that this support provides to the Mn-based sorbent [14], combined with other properties such as its mechanical strength and ease of modification. Mo is selected as the promoter to further improve the performance of Mn-alumina sorbents, in terms of stability and capacity. In order to investigate the potential of this system, we report on a series of Mn-based sorbents that are synthesized with various amounts of Mo addition. All samples are first tested for high-temperature desulphurization with several sorption/regeneration cycles. Characterization by means of fundamental methods is also presented here which allows evaluating the material properties relevant for the sorption as well as the changes induced by the multiple sorption/regeneration cycles.

2. Methods and experimental

2.1. Chemicals

All chemicals and gases were applied as received without any further processing. The support, γ-alumina LOT#B5160010 with purity 96%, was obtained from Strem chemicals. Manganese precursor, manganese nitrate (Mn(NO3)2·4H2O), and molybdenum precursor, ammonium molybdate ($(NH_4)_6Mo_7O_{24}\cdot 4H_2O$) were purchased from Sigma Aldrich.

2.2. Sample preparation

The alumina support was pre-calcined in a muffle furnace at 500 °C for 10 h with air before being impregnated with Mn and/or Mo precursors. All sorbents were synthesized by the wet impregnation method with γ-alumina support, deionized water, Mn and/or Mo precursors. Following the impregnation, the samples were aged overnight and then dried at 90 °C for 24 h. All dried samples were subsequently calcined at 600 °C in flowing air for 5 h, followed by crushing and sieving to the desired size range, 150–250 μm. The nominal Mn loading for all samples is 15 wt%, and the Mo loadings are 0, 2, 5, and 8 wt%, with corresponding sample names 15Mn, 15Mn2Mo, 15Mn5Mo and 15Mn8Mo, respectively. The regenerated samples after repeated sorption and regeneration cycles are marked with an affix –AR, e.g. 15Mn8Mo-AR.

2.3. Instrumentation and methods

Nitrogen adsorption-desorption isotherms were measured with a Micromeritics TriStar 3020 instrument. Samples were degassed at 200 °C for 12 h in advance of the corresponding measurements. The specific surface area of the samples was evaluated by the Brunauer-Emmett-Teller (BET) method in the range of relative pressures $p/p_0 = 0.1–0.3$. The pore size distributions were obtained from the desorption branch of the isotherm using the Broekhoff-DeBoer algorithm [27].

X-ray diffraction analysis (XRD) of the solid sorbents were conducted on a Bruker AXS D8 Focus diffractometer using CuK_α radiation ($\lambda = 1.54$ Å). The crystallite size of the active phase was calculated by the Scherrer equation (Equation (6)) [28]:

$$\tau = \frac{K\lambda}{\beta \cos\theta} \tag{6}$$

where the shape factor, K, is applied as 0.9. Raman spectroscopy measurements were performed on a Horiba Jobin Yvon, LABRAM HR 800 instrument. A laser excitation source of 633 nm was used and focused with a 50 × objective. UV–vis spectroscopy measurements were conducted on an Avaspec-3648 UV–visible spectrophotometer (Avantes, Netherlands) in the light wavelength range of 250–850 nm.

The sulfur sorption tests were conducted in an in-house built laboratory setup consisting of a gas feeding and metering system, a quartz fixed bed reactor with an inner diameter of around 6 mm, and an analytical sections using a quadrupole mass spectrometer to continuously monitor the concentrations of all gas compositions, especially H_2S, see Ref. [25] for further details. The composition of the off-gas from the reactor was measured continuously by a ThermoStar GSD 320 T1 C analytical system equipped with a quadrupole mass spectrometer QMS 200 using a secondary electron multiplier detector. A sample mass of 0.2 g of sorbent which constitutes a bed height of around 8–10 mm was used for all performance tests. Prior to the sorption experiment, the sample was reduced in-situ with a H_2/N_2 gas mixture (50 mL/min with 50 vol% H_2), with a heating rate of 15 K/min to reach the sorption temperature, 600 °C, and holding for 1 h. After the reduction, the system was flushed with N_2 until no H_2 was detected by the MS. The sorption gas was subsequently introduced to the bypass line for 25 min in order to stabilize the MS signals before the gas was directed to the reactor for the sorption process. The feed gas composition for the sorption experiments was 0.4, 39.6, 40.0 and 20 vol% for H_2S, Ar, H_2 and N_2, respectively. A rather high H_2S concentration was used in order to accelerate the experiments and facilitate a large number of sorption/regeneration cycles during the testing period. When the breakthrough H_2S was observed, defined as when the exit gas concentration increased to 40 ppm above the lowest level, the sorption cycle was terminated by flushing the reactor with N_2. Then the sample was heated to 650 °C and stabilized with flowing N_2 for 10 min. The regeneration was then initiated, by switching to a gas mixture containing 25 vol% air diluted with N_2. This leads to the formation of SO_2. The regeneration was terminated by flushing the reactor with N_2 when the SO_2 signal was relaxed back to the baseline, typically after around 15 min. The total gas flow used for the sorption and regeneration was 100 mL/min for all gas compositions, corresponding to a space velocity of 10,000 hr^{-1}, and all experiments were done at 1 bar total pressure.

The residual amounts of components present in the outlet gas was measured quantitatively based on a regular calibration of the MS signals. The curve expressing the concentration of outlet H_2S versus time is used to determine the sorbent capacity before the breakthrough at these conditions. The breakthrough capacity (BC) is defined as the amount of sulfur removed by the sorbent before reaching the breakthrough, and this was calculated from a simple mass balance. The BC was calculated by the following formula (Equation (7)):

$$BC\left(\frac{g\ of\ H_2S}{g\ of\ sorbent}\right) = \frac{Q \times \int_0^t (c_{in} - c_{out}) \times M_{H_2S}}{24.04 \times 10^9 \times m_s} \tag{7}$$

where Q is the flow rate of the gas mixture, i.e. 100 mL/min; C_{in} and C_{out} are the inlet and outlet concentration of H_2S (ppm); m_s is the mass of the loaded solid sorbent, 0.2 g, and M_{H2S} is the molecular weight of H_2S.

The O_2 and SO_2 concentration during the regeneration was monitored only qualitatively following the m/z values of O_2 and SO_2. N_2 contained in the model gas mixture was used as an internal standard to calibrate the MS, while the second inert gas, Ar, was just used to dilute H_2S in the supplied gas mixture (1 vol% H_2S in Ar).

Each performance test of samples was conducted for 10 repeated sorption/regeneration cycles. In between each sorption/regeneration cycle, the system was flushed with N_2. During the longer breaks between the cycles (overnight), the system was kept under N_2/H_2 flow at the reaction temperature. The total flow, in this case, was 40 mL/min, and the gas composition was the same as used in the pre-reduction step, i.e. 50 vol% of H_2 in N_2.

2.4. Thermodynamic calculations

The Equilib module in the Factsage™ software package 7.0 (GTT Technologies) was applied to calculate the theoretical residue of sulfur concentration in the gas phase in a user-specified state point. Husmann and co-authors utilized the method to evaluate the performance of different sorbent materials for in-situ desulphurization of biomass-derived synthesis gas [29]. Through Factsage calculations, they acquired phase equilibrium calculations for the H_2S equilibrium concentration with various parameters. In this study, we adapted the same method (details in Refs. [29]) and modeled the gas with the same composition, containing 29 vol% H_2, 16 vol% CO_2, 8 vol% CO, 4 vol% CH_4, 4 vol% N_2, 38 vol%H_2O, and 15 ppmv H_2S. In order to calculate the equilibrium content of H_2S in the presence of metal-based sorbents under dry gas conditions, the input value of H_2S is raised to 1400 ppm, and the steam content is converted to inert gas content, N_2. The most common metals studied for high-temperature desulphurization – i.e. Zn, Cu, Mn, Ca, Fe, Mo, – are evaluated here under such a gas mixture in the temperature range of 300–1000 °C, which covers the mid-to high--temperature desulphurization processes. The resulting residual H_2S concentrations at equilibrium are shown in Fig. 1, and the calculated distribution of solid phases are shown in Appendix A-supplementary information. The residual values of H_2S for all of these metal oxides increases gradually with increasing temperature. In terms of the H_2S residual level, CaO, CuO and ZnO exhibit excellent H_2S elimination capacity, however, they have their own drawbacks [6,7]. It is difficult to regenerate CaO at mild conditions, and this limits its application for a chemical looping desulphurization process [6]. The H_2S residue level after treatment with CuO is as low as the sub-ppm level, however, at temperatures higher than 450 °C, most of the sulfur species are converted to SO_2, which is highly corrosive, especially when a high steam content is present. SO_2 can also react with H_2S forming elementary sulfur, potentially causing blockage of the equipment. Another drawback for CuO is its low resistance toward reduction and volatilization under syngas and such temperature conditions, due to the formation of Cu_2O and metallic Cu and loss of desulphurization capacity [6]. ZnO has similar issues related to volatilization and sulfate formation at temperatures higher than 400 °C [6]. MnO, FeO and MoO_2, in contrast, show higher H_2S equilibrium values, varying from 10 to 100 ppm at temperatures below 600 °C. However, Mn oxide is commonly recognized as a better candidate for sorbent desulphurization at temperatures higher than 500 °C. It also converts most of the sulfur species to the solid phase, which potentially reduces the blockage issues caused by SO_2 and H_2S reacting to form elemental sulfur [6]. The solid compositions at the equilibrium of the oxides are listed in Table S1 in the Appendix, which

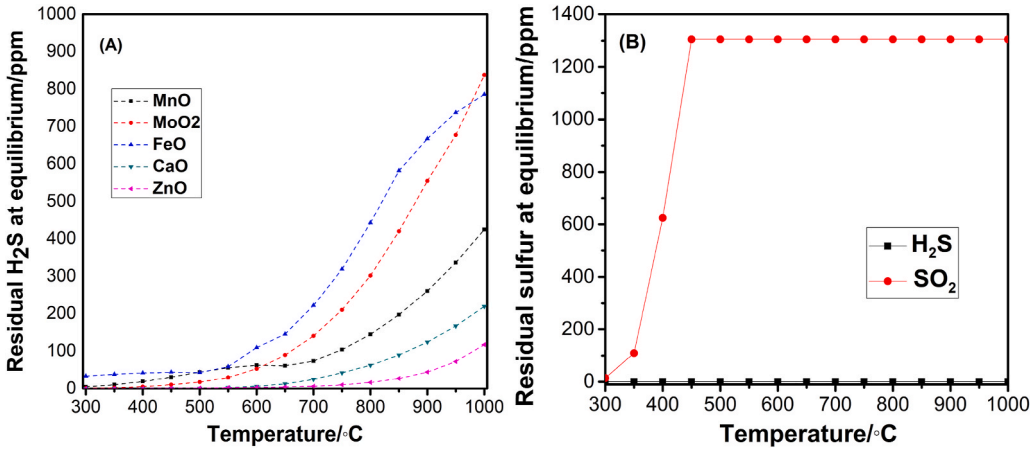

Fig. 1. Calculated **theoretical** values of H_2S equilibrium concentration for metal sorbents as a function of temperature ranging from 300 to 1000 °C. The data points were computed for every 50 °C considering all potential reactions. The input gas mixture is 29 vol% H_2, 16 vol% CO_2, 8 vol% CO, 4 vol% CH_4, 42 vol% N_2 and 1400 ppmv H_2S. (A): H_2S levels for MnO, MoO_2, FeO, CaO and ZnO; (B): H_2S and SO_2 levels for CuO.

also demonstrates that the H_2S converted by MnO is retained in the solid phase as MnS.

3. Results and discussion

3.1. Mo addition

Experimental data acquired from the Mn-based solid sorbents under 10 repeated sulphidation/regeneration cycles experiments are shown in Fig. 2. Addition of Mo to the Mn-based solid sorbents increases the initial capacity of these sorbents, compared to the reference sorbent, the unpromoted 15Mn, as shown in Fig. 2A. This observation is partially related to the activity of molybdenum oxide itself, contributing to removing H_2S from the syngas stream by chemical sorption according to reaction 1. The theoretical capacities of all sorbent are calculated by assuming all metal oxides, both Mn and Mo, are converted to sulfide, and the values are included in Fig. 2A. The ratio between the measured initial capacity to the theoretical capacity of each sorbent declined with increasing Mo-addition, suggesting lower efficiency of usage of metal oxides. However, when fairly large amounts of Mo are added we observe a significant improvement of the Mn-based sorbents. For example, the capacity for the 15Mn2Mo sorbent in the successive cycles declined significantly, with worse stability compared with sorbents with larger amounts of Mo added. (see Fig. 2B). Further increasing the Mo content from 2 to 5, and 8 wt%, substantially enhances the stable sorption capacity after successive cycles.

Regarding the stability, the unpromoted Mn sample, 15Mn, showed a sharp capacity decline between the first and second sorption cycle. After 10 repeated sorption and regeneration cycles, 57% of the initial capacity was retained, which was similar to a previous study [14]. For the 15Mn2Mo sorbent, the sorption capacity also showed an obvious decline for the second cycle. In contrast, for the 15Mn5Mo and 15Mn8Mo sorbents, it increased measurably. Both these sorbents exhibited good stabilities after the second sorption. The comparison of the ratio of capacities between the highest observed value and 10th cycles are summarized in Table 1.

As shown in Fig. 2B, the capacity for all sorbents is substantially lower in the 5th cycle, which is recorded following an extended period (overnight) when the sorbent sample is kept at 600 °C in a reducing atmosphere. However, after a subsequent sorption and regeneration

Table 1
Comparison of the ratio between the capacity in the 10th cycle and the highest observed capacity for all sorbents.

Sorbent code	Cycle with highest capacity	Capacity loss
15Mn	1	44
15Mn2Mo	1	28.5
15Mn5Mo	1	18.3
15Mn8Mo	2	9.7

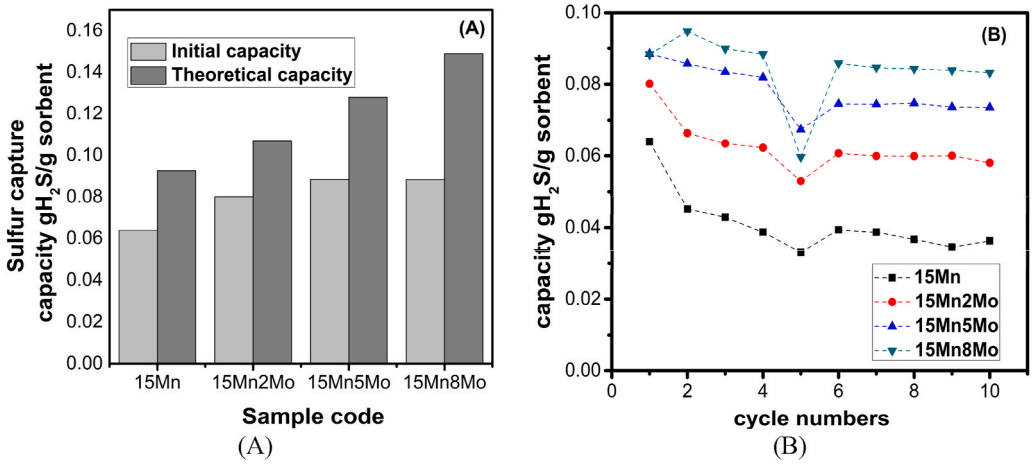

Fig. 2. (A) Initial sulfur removal capacity and theoretical capacity of each sample (B) capacity for each sorption cycle during performance test on all samples.

cycle, for all the sorbents most of the capacity is recovered and the capacity trend follows that we observed before the overnight period. Such a temporary loss of the sorbent's performance due to the overnight treatment was also previously reported for the Mn_xO_y-Al_2O_3 sorbent in our group [25]. This is probably due to a partial reduction during the period overnight in a reducing atmosphere, either reducing the capacity or blocking the initial steps of the sorption and decomposition of H_2S on the surface. This effect is completely reversed following a complete cycle.

A possible explanation is that the H_2 treatment forms species on the surface with fewer active sites for the interaction with H_2S, or simply that the extended exposure to a reducing atmosphere leads to a partial reduction of the manganese oxide, thus reducing the uptake capacity. However, with the subsequent oxidation treatment during the regeneration cycle, the effect is reversed. It is worth mentioning that the capacity lost after overnight for the 15Mn8Mo sorbent was much larger than that of the other sorbents. This together with the lower 1st cycle capacity (following a pre-reduction of the material) compared to the capacities of successive cycles, suggest that the H_2 treatment may somehow interfere with the Mn–Mo structures, which probably are active for the H_2S removal. This will be further discussed in the characterization part.

3.2. Characterization

3.2.1. N_2 adsorption measurement

The textural properties of fresh and reacted sorbents promoted with molybdenum are analyzed by nitrogen adsorption, and the results are shown in Table 2. The addition of Mo resulted in a slightly increased surface area, however, the effect is limited and within the experimental error. The average pore width varies around 14 nm, and the pore volumes are around 0.5 cm^3/g, thus, both properties are very similar to the unpromoted sample, 15Mn, as presented in Table 2. In general, the promotion with small loadings of Mo, between 2 and 8 wt%, causes only minor changes in the textural properties, hence, the main features of the unpromoted sample like the high surface area, and the proper pore system.

The sorption-regeneration experiments, however, lead to significant changes in the textural properties of the samples, including a decrease in the surface area, an enlargement of the pore widths, and a loss of pore volume. By increasing the Mo-loading, the surface area of the regenerated samples decreases to a larger degree than the unpromoted sample, 15Mn, as also indicated in Table 2. These changes in textural properties are due to the sintering process at the applied temperatures of 600 °C during sorption and particularly at 650 °C during regeneration with air. Sintering is associated with shrinking of the pore volume and increasing the average pore width, resulting from loss of micropores. The observed changes in the textural properties of the regenerated sorbents appear to increase with the Mo loading. This is a curious observation, since increasing Mo-addition also leads to increased stability of the sorption capacity. This would indicate that the loss of the sorption capacity is not related to overall morphological changes in the material, but rather other changes, e.g. chemical reactions forming non-reactive species.

Table 2
Textural properties of fresh and regenerated sorbents upon multiple sorption/regeneration cycles.

Sorbent	Surface area [m^2/g]	Average pore width [nm]	Pore volume [cm^3/g]
15Mn	121	14.1	0.47
15Mn2Mo	130	14.2	0.52
15Mn5Mo	122	12.9	0.42
15Mn8Mo	125	13.9	0.48
15Mn-AR	115	15.7	0.52
15Mn2Mo-AR	98.2	16.8	0.48
15Mn5Mo-AR	91.8	16.7	0.40
15Mn8Mo-AR	85.3	17.4	0.41

3.2.2. X-ray diffraction (XRD)

Chemical phases present in the investigated samples were identified by X-ray powder diffraction and spectra of fresh and regenerated sorbents are given in Fig. 3.

As shown in Fig. 3A, the phases of Mn_2O_3 and/or $MnMoO_4$ can be observed on fresh sorbents in addition to the diffraction pattern of the γ-alumina support. Two intense peaks at a 2θ angle of approximately 46° and 67° are assigned to γ-alumina and is present in the XRD patterns of every sample. Besides γ-alumina, the unpromoted sample, 15Mn, shows peaks for the phase of Manganese (III) oxide, Mn_2O_3, at approx. 23°, 33°, 38°, 49°, and 55°, which can also be identified in the other samples with Mo-addition. In XRD patterns of the sample with Mo addition, peaks assigned to the phase $MnMoO_4$ emerge at 2θ angles of 22.5°, 26°, 26.5°, 27.5° and 31°. With increasing Mo-loading, these sharp and narrow peaks of $MnMoO_4$ are gaining in intensities.

On regenerated samples the reflections of γ-alumina, Mn_3O_4, and $MnMoO_4$ are identified after ten successive sorption/regeneration cycles, as depicted in Fig. 3B. Besides the peaks of γ-alumina at 2θ angles of approximately 37°, 46°, and 67°, the unpromoted sample 15Mn-AR shows peaks for the hausmannite phase of (Manganese (II,III) oxide, Mn_3O_4) at 2θ angles of approximately 18°, 29°, 32.5°, 36°, 44°, 50.5°, 58.5°, 60° and 64.5°. These peaks are observed for all regenerated sorbents promoted with molybdenum.

For 15Mn2Mo-AR, the obtained peaks of Mn_3O_4 appear broader and less sharp indicating a lower crystallinity or smaller particles. Peaks at 2θ angles of approximately 22.5°, 24.5°, 26°, 26.5°, 27.5°, 31°, and 33° correspond to the presence of $MnMoO_4$, No single Mo oxide was observed, indicating the Mo is mainly present as $MnMoO_4$ or in amorphous phasesIn the diffractogram of 15Mn5Mo-AR, the peaks of $MnMoO_4$ are more intense compared to the samples with less Mo, whereas the diffraction peaks of hausmannite and γ-Al_2O_3 remain nearly unchanged compared to 15Mn2Mo-AR. Apparently, a minimum amount of molybdenum is required to sufficiently stabilize the manganese oxide in form of MnMoO4, which in principle is a combination of the most stable manganese and molybdenum oxides and can be converted to Mn and Mo oxides under the reducing syngas environment as shown in reaction (8).

$$MnMoO_4 + H_2 \rightarrow MnO + MoO_2 + H_2O \quad (8)$$

It can be speculated that the higher amount of crystalline $MnMoO_4$, as the main difference between the XRD patterns of 15Mn2Mo-AR and 15Mn5Mo-AR, is responsible for the improved sorption capacity and enhanced stability. The increased amount of crystalline manganese (II) molybdate also enhances the initial capacity, as shown in Fig. 2A.

For 15Mn8Mo-AR, these changes and effects are also present. The higher Mo-loading of 8 wt% results in a strongly increased relative intensity, comparing to characteristic peaks of alumina, of the main peak of MnMoO4 at the 2θ angle of approximately 26°. The increment also appears for the other characteristic peaks, however, less obvious. Therefore, the enhanced amount of crystalline manganese (II) molybdate appears to stabilize a larger amount of manganese oxide, which is reflected by the significantly improved sorption capacity and stability of 15Mn8Mo. It is noticeable that a reduced relative intensity of the diffraction peaks of hausmannite can be observed in the diffractogram, possibly contributing to the improved sorption behavior.

For all sorbents, the crystallite size of the active phase calculated by the Scherrer equation is presented in Table 3. Either the most obvious characteristic peaks for corresponding compounds or the peaks without overlapping with other peaks were selected for the calculation. The 2θ peak at 33° was chosen for Mn_2O_3, 36° for Mn_3O_4 and 26° for $MnMoO_4$. Although no large difference is observed between the unpromoted

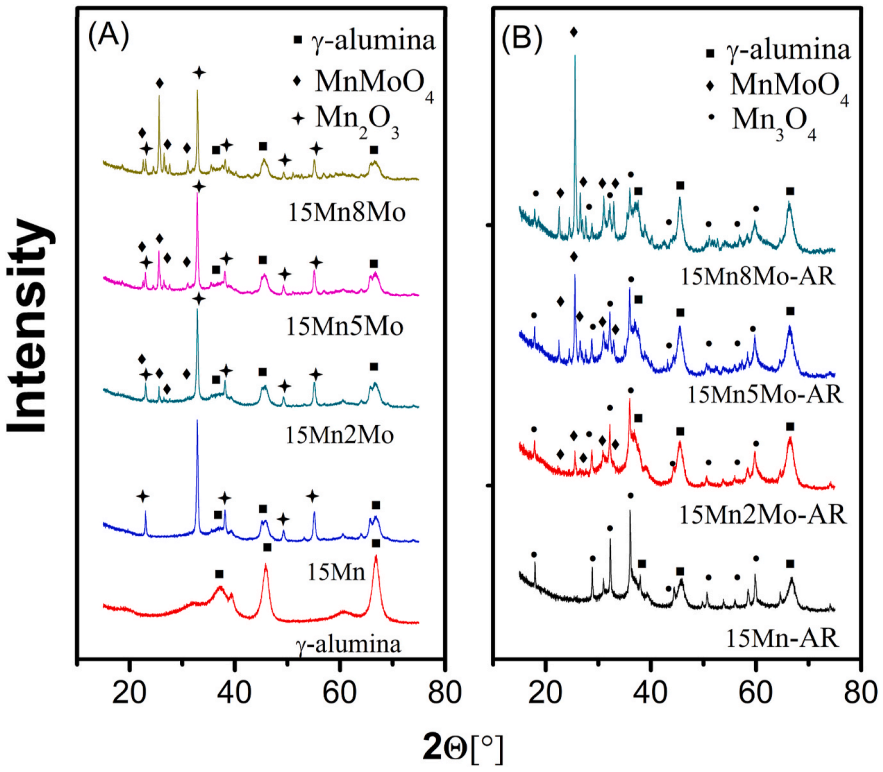

Fig. 3. XRD patterns for the support material, fresh sorbents (A) and spent sorbents (B) after 10 repeated sorption/regeneration cycles. ●: Mn_3O_4; □: Mn2O3; □: MnMoO4; ■: γ-alumina.

Table 3
Crystallite sizes of species existing on samples calculated by Scherrer equation. The selected.

Sorbent codes	Crystallite Size/nm		
	Mn_2O_3 at 2θ = 33°	Mn_3O_4 at 2θ = 36°	$MnMoO_4$ at 2θ = 26°
15Mn	27	–	–
15Mn2Mo	27	–	55
15Mn5Mo	28	–	38
15Mn8Mo	31	–	40
15Mn-AR	–	37	
15Mn2Mo-AR	–	32	50
15Mn5Mo-AR	–	30	40
15Mn8Mo-AR	–	32	43

sample and 15Mn2Mo, the manganese (III) oxide phase Mn_2O_3 shows a slight increase in crystallite size with increasing Mo-loading for the fresh sorbents. 15Mn8Mo shows the largest crystallite size, 31 nm. The crystalline particles of $MnMoO_4$ are larger in size, ranging from 55 nm for the sample 15Mn2Mo and around 40 nm for the samples with higher Mo-loading.

After ten successive sorption-regeneration cycles the manganese oxide phase of Mn_2O_3 is transformed to Mn_3O_4, as described above. This phase transformation is accompanied by a general increase in crystallite size, the crystals are now in the range 30–37 nm. For 15Mn2Mo, the Mn oxide species dominate compared to Mo-containing phases, and the growth of the Mn oxide particle size could be an explanation for the observed deactivation, in that the core of the oxide particle remains unreacted (shrinking core). When the particle grows bigger the distance the sulfur has to diffuse into the oxide particle, and correspondingly; the distance the oxygen needs to diffuse out, increases, leaving a larger fraction of the core unreacted. The crystallite size of $Mn(MoO_4)$ remained relatively constant for samples with 5 wt% and 8 wt% of molybdenum, even decreased slightly for15Mn2Mo following 10 cycles, which could explain the apparent stability of the Mn–Mo containing materials. It can be suggested that the formation of the Mn–Mo mixed phase, $MnMoO_4$, promotes the stability of the Mn species and adding more Mo enhances the effect. The present work is limited to studying 10 sorption-regeneration cycles, and the results indicate a good long-term stability of this system. The loss in capacity is very small over the last 4 cycles. Taking into account that the conditions here are accellerated (using a high H_2S concentration), suggests that this sorbent system has the potential to be applied for a cyclic gas cleaning operation.

3.2.3. *Raman spectroscopy*

Raman spectroscopy is utilized in this study as a tool to investigate the surface and subsurface properties of the prepared solid sorbents. This technique serves as a complementary method to XRD which provides information about the bulk properties of the sorbents. Raman spectra of reference Mn oxides and the alumina-supported Mn-based sorbents have previously been recorded in our group [14,26]. Mn_3O_4 was found to be the most Raman active phase with a peak at approx. 667 cm-1 MnO_2 and Mn_2O_3 reference oxides were reported to be less Raman active, however, some characteristic spectral features were recognized for MnO_2 and Mn_2O_3 oxides at 656 cm^{-1} and 708 cm^{-1}, respectively. γ-Alumina did not show any characteristic peaks in the examined region of 200–1000 cm^{-1}. This information will be utilized here as a guide to examine the prepared solid sorbents, and also to study the effects of Mo addition in the crystalline structure of the Mn-based sorbents.

Raman spectra of the fresh and regenerated Mn-based solid sorbents, together with the Mo-promoted sorbents are shown in Fig. 4. Compared with the unpromoted 15Mn–Al_2O_3 sample reported previously [14], the freshly prepared unpromoted 15Mn sorbent exhibited different Raman characteristic features, i.e. no characteristic peaks for the Mn_3O_4 oxide is observed in the spectra. This might be due to the higher calcination temperature utilized in the current study. The main peak detected at 350

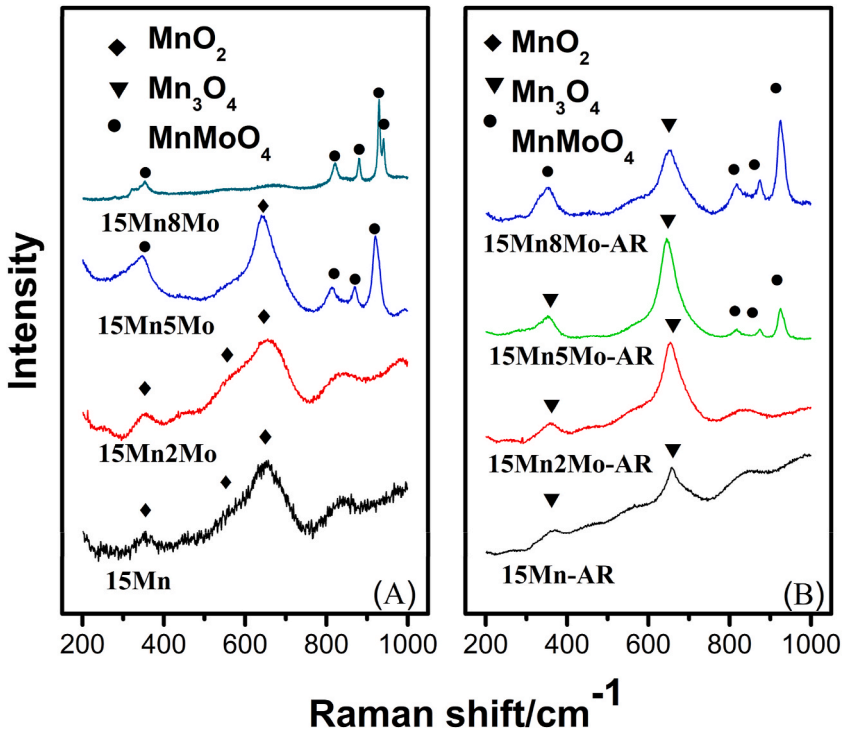

Fig. 4. Raman spectra of the fresh (left) and regenerated sorbents (right) after 10th sorption cycles.

[30] and 650 cm^{-1} along with a shoulder at 573 cm^{-1} may be assigned to MnO_2, which is not detected in XRD and assumed to be amorphous. The weak shoulder at around 704 cm^{-1} reflects the presence of Mn_2O_3.

The addition of a small amount of Mo, sample 15Mn2Mo, causes a small shift in the Raman features of sorbents comparing to the unpromoted sample, 15Mn. As discussed with the XRD data, the $MnMoO_4$ structure forms with the addition of Mo, and the main Raman characteristic features assigned to this structure are peaks positioned at 282, 290, 337, 354, 820, 884, 931 and 943 cm^{-1} [22]. As shown in Fig. 4, by increasing the amount of Mo to the sorbent samples, from 2 to

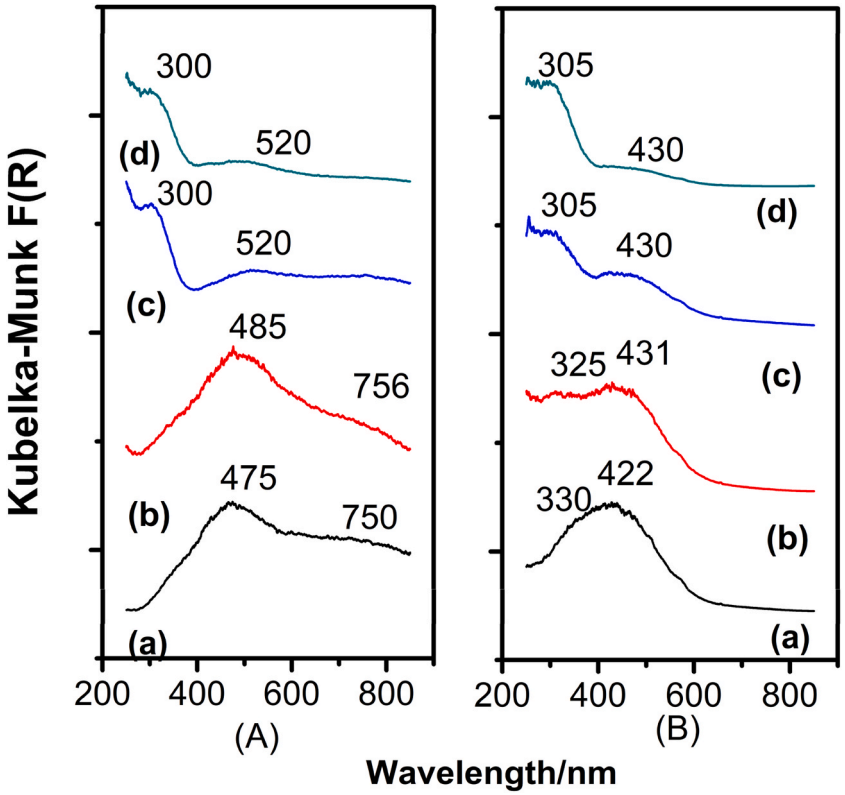

Fig. 5. UV–vis DRS of the (A) fresh and (B) regenerated samples, (a) 15Mn; (b) 15Mn2Mo; (c) 15Mn5Mo and (d) 15Mn8Mo.

8 wt%, the peak characteristics for the $MnMoO_4$ structure emerge and become clearer and sharper, which are in agreement with the results from XRD.

After going through the performance cycling tests, the regenerated samples showed different Raman characteristic features (see Fig. 4B). The spectrum of the unpromoted sample, 15Mn, now exhibited peaks at 660 and 370 cm^{-1}, corresponding to Mn_3O_4. With a low Mo addition, the 15Mn2Mo-AR650 sample, the Raman characteristic peaks are similar to those of the unpromoted sample, 15Mn-AR650. However, with higher Mo addition, new peaks are detected at 928, 874, 820 and 353 cm^{-1}, which again indicates the presence of the $MnMoO_4$ species. These peaks are more intense for the 15Mn8Mn-AR sorbent and may be linked to the additional stability provided by the higher Mo-addition. Furthermore, following regeneration, a significant peak at 650 cm^{-1} with a small shoulder at 580 cm^{-1} indicates the presence of MnO_2. The peak at 353 cm^{-1} became broader and a shoulder at 331 cm^{-1} may reveal the presence of Mn_3O_4.

3.2.4. UV–vis

UV–vis spectroscopy is an efficient tool to distinguish the valence state of species and their chemical environment. The application of UV–vis spectroscopy in research on heterogeneous materials is related to the study of transition metal ion (TMI) centers, rare earth metal ions < adsorbed molecules, molecular ions, and radicals [20,22].

UV–vis spectra of Mn-based sorbents with Mo-addition are shown in Fig. 5. Mn-containing materials have been investigated previously, as a single-phase [31], as binary oxide systems [32,33] or as triplex systems [20]. The spectrum of the fresh unpromoted sorbent, 15Mn, presents two main absorption bands at 475 and 750 nm, which both are assigned to the d-d transition of Mn^{3+} [33]. This is consistent with the characterization results from XRD and Raman, which both indicate that Mn is present in the fresh sample in the form of Mn_2O_3. By adding a small amount of Mo, 15Mn2Mo, these peaks are shifted to slightly higher wavelengths, compared with the unpromoted sample, which indicates that the interaction with the Mo species enhances the bandgap energy of the Mn species [17]. There are no characteristic bands observed for Mo oxides in the 15Mn2Mo sample, which may imply that the Mo species are not present on the outermost surface of the materials, or that the concentration is too low to be detected. However, sorbents with a higher amount of Mo addition, i.e. 15Mn5Mo and 15Mn8Mo, show less significant characteristic features for Mn oxides, but weak absorption bands at 520 and 760 nm related to Mn^{2+} and Mn^{3+} are visible. These bands are even weaker for the 15Mn8Mo sorbent, confirming the transition to the manganese molybdate compound. Additionally, a strong absorption appeared in the UV region with a peak at 300 nm for both 15Mn5Mo and 15Mn8Mo sorbents. This can be explained by the charge transfer of O^{2+} to Mo^{3+} [34,35] and confirms a well-developed $MnMoO_4$ structure.

For the regenerated samples, the band positions for the unpromoted sample, 15Mn, are shifted to lower wavelengths. Sample 15Mn-AR shows a broadband at 422 nm, which is assigned to MnO_2 [20,33]. A shoulder at 330 nm can be assigned to charge transfer from O^{2-} to Mn^{3+} in Mn_3O_4 [20,33]. A clearer absorption peak present at approx. 325 nm for the 15Mn2Mo sample is suggested to be due to the formation of more Mn_3O_4 on the sample. This indicates that Mo addition helps to retain a lower oxidation state of Mn, and a smaller particle size of Mn species [20]. Moreover, the absorbance in the lower wavelength area (around 300 nm) also increases, which may be assigned to Mo species. The weak characteristic band for manganese oxide on 15Mn5Mo shifts to slightly lower wavelength at 430 nm, suggesting the transition of Mn oxides from Mn_2O_3 to Mn_3O_4 [33]. The absorption in the UV region, mainly wavelength around 305 nm, remains high, which indicates that $MnMoO_4$ is preserved and it is stable after repeated desulphurization cycles. It is worth mentioning that the smaller variation in the spectra of the fresh and spent 15Mn8Mo sorbent illustrates the stability of this sample, due to the significant role of the Mo addition in this respect.

4. Summary and conclusions

A series of Mn-based desulphurization sorbents with different amounts of Mo addition were prepared, characterized, and tested for H_2S sorption and regeneration. The sorbent with the largest Mo-addition, 15Mn8Mo, exhibited improved and promising performance regarding sorption capacity and stability. Formation of the mixed oxide, $MnMoO_4$, is proposed to play a role in promoting the sorbent. Comparing to the unpromoted sorbent 15Mn, the promoted sorbent 15Mn8Mo showed a 38% increase of the initial capacity and significantly less deactivation, with only 9.7% capacity loss after 10 sorption/regeneration cycles. This shows that the material is well suited as a regenerable sorbent in a chemical looping sorption process.

Acknowledgments

The Norwegian Research Council is gratefully acknowledged for financial support through contracts 267986 and 257622.

Appendix A. Supplementary data

Supplementary data to this article can be found online at https://doi.org/10.1016/j.biombioe.2020.105843.

References

[1] G.W. Huber, S. Iborra, A. Corma, Synthesis of transportation fuels from biomass: chemistry, catalysts, and engineering, Chem. Rev. 106 (2006) 4044–4098, https://doi.org/10.1021/cr068360d, 106.
[2] S.S. Tamhankar, M. Hasatani, C.Y. Wen, Kinetic studies on the reactions involved in the hot gas desulfurization using a regenerable iron oxide sorbent—I: reduction and sulfidation of iron oxide, Chem. Eng. Sci. 36 (1981) 1181–1191, https://doi.org/10.1016/0009-2509(81)85066-X.
[3] N. Abdoulmoumine, S. Adhikari, A. Kulkarni, S. Chattanathan, A review on biomass gasification syngas cleanup, Appl. Energy 155 (2015) 294–307, https://doi.org/10.1016/j.apenergy.2015.05.095.
[4] L. Wang, J.E. Hustad, Ø. Skreiberg, G. Skjevrak, M. Grønli, A critical review on additives to reduce ash related operation problems in biomass combustion applications, Energy Procedia 20 (2012) 20–29, https://doi.org/10.1016/j.egypro.2012.03.004.
[5] A.H. Lillebø, A. Holmen, B.C. Enger, E.A. Blekkan, Fischer-Tropsch conversion of biomass-derived synthesis gas to liquid fuels, Wiley Interdiscip. Rev. Energy Environ. 2 (2013) 507–524, https://doi.org/10.1002/wene.69.
[6] S. Cheah, D.L. Carpenter, K.A. Magrini-Bair, Review of mid- to high-temperature sulfur sorbents for desulfurization of biomass- and coal-derived syngas, Energy Fuels 23 (2009) 5291–5307, https://doi.org/10.1021/ef900714q.
[7] X. Meng, W. De Jong, R. Pal, A.H.M. Verkooijen, In bed and downstream hot gas desulphurization during solid fuel gasification: a review, Fuel Process. Technol. 91 (2010) 964–981, https://doi.org/10.1016/j.fuproc.2010.02.005.
[8] H.H. Kung, Deactivation of methanol synthesis catalysts - a review, Catal. Today 11 (1992) 443–453, https://doi.org/10.1016/0920-5861(92)80037-N.
[9] H. Boerrigter, H. Den Uil, H.-P. Calis, Green Diesel from Biomass via Fischer-Tropsch Synthesis: New Insights in Gas Cleaning and Process Design, in: Paper presented at: Pyrolysis and Gasification of Biomass and Waste, Expert Meeting, 30 September - 1 October 2002, Strasbourg, France, 2002.
[10] H. Leibold, A. Hornung, H. Seifert, HTHP syngas cleaning concept of two stage biomass gasification for FT synthesis, Powder Technol vol. 180 (2008) 265–270, https://doi.org/10.1016/j.powtec.2007.05.012.
[11] P.J. Woolcock, R.C. Brown, A review of cleaning technologies for biomass-derived syngas, Biomass Bioenergy 52 (2013) 54–84, https://doi.org/10.1016/J.BIOMBIOE.2013.02.036.
[12] P.R. Westmoreland, D.P. Harrison, Evaluation of candidate solids for high-temperature desulfurization of low-btu gases, Environ. Sci. Technol. 10 (7) (1976) 659–661, https://doi.org/10.1021/es60118a010.
[13] W.F. Elseviers, H. Verelst, Transition metal oxides for hot gas desulphurisation, Fuel 78 (1999) 601–612, https://doi.org/10.1016/S0016-2361(98)00185-9.
[14] S. Chytil, M. Kure, R. Lødeng, E.A. Blekkan, Performance of Mn-based H_2S sorbents in dry, reducing atmosphere – manganese oxide support effects, Fuel 196 (2017) 124–133, https://doi.org/10.1016/j.fuel.2017.01.087.
[15] T.-H. Ko, H. Chu, Y.-J. Liou, A study of Zn–Mn based sorbent for the high-temperature removal of H_2S from coal-derived gas, J. Hazard Mater. 147 (2007) 334–341, https://doi.org/10.1016/J.JHAZMAT.2007.01.018.
[16] J. Zhang, Y. Wang, D. Wu, Effect investigation of ZnO additive on Mn-Fe/γ-Al2O3 sorbents for hot gas desulfurization, Energy Convers. Manag. 44 (2003) 357–367, https://doi.org/10.1016/S0196-8904(02)00068-7.
[17] F.M. Zhang, B.S. Liu, Y. Zhang, Y.H. Guo, Z.Y. Wan, F. Subhan, Highly stable and regenerable Mn-based/SBA-15 sorbents for desulfurization of hot coal gas,

J. Hazard Mater. (2012) 233–234, https://doi.org/10.1016/J.JHAZMAT.2012.07.023, 219–227.
[18] Z.F. Zhang, B.S. Liu, F. Wang, S. Zheng, High-temperature desulfurization of hot coal gas on Mo modified Mn/KIT-1 sorbents, Chem. Eng. J. 272 (2015) 69–78, https://doi.org/10.1016/J.CEJ.2015.02.091.
[19] D. Wang, J. Yu, L. Chang, D. Wang, Effects of addition of Mo on the sulfidation properties of Fe-based sorbents supported on fly ash during hot coal gas desulfurization, Chem. Eng. J. 166 (2011) 362–367, https://doi.org/10.1016/J.CEJ.2010.11.008.
[20] H. Xia, B. Liu, Q. Li, Z. Huang, A.S.-C. Cheung, High capacity Mn-Fe-Mo/FSM-16 sorbents in hot coal gas desulfurization and mechanism of elemental sulfur formation, Appl. Catal. B Environ. 200 (2017) 552–565, https://doi.org/10.1016/J.APCATB.2016.07.053.
[21] B. Guan, W. Sun, Y. Wang, Carbon-coated $MnMoO_4$ nanorod for high-performance lithium-ion batteries, Electrochim. Acta 190 (2016) 354–359, https://doi.org/10.1016/J.ELECTACTA.2016.01.008.
[22] C. Sekar, R.K. Selvan, S.T. Senthilkumar, B. Senthilkumar, C. Sanjeeviraja, Combustion synthesis and characterization of spherical α-$MnMoO_4$ nanoparticles, Powder Technol. 215–216 (2012) 98–103, https://doi.org/10.1016/J.POWTEC.2011.09.016.
[23] S.-S. Kim, S. Ogura, H. Ikuta, Y. Uchimoto, M. Wakihara, Reaction mechanisms of $MnMoO_4$ for high capacity anode material of Li secondary battery, Solid State Ionics 146 (2002) 249–256, https://doi.org/10.1016/S0167-2738(01)01013-X.
[24] W.J. Bakker, F. Kapteijn, J.A. Moulijn, A high capacity manganese-based sorbent for regenerative high temperature desulfurization with direct sulfur production: conceptual process application to coal gas cleaning, Chem. Eng. J. 96 (2003) 223–235, https://doi.org/10.1016/J.CEJ.2003.08.022.
[25] S. Chytil, M. Kure, R. Lødeng, E.A. Blekkan, On the initial deactivation of Mn_xO_y–Al_2O_3 sorbents for high temperature removal of H_2S from producer gas, Fuel Process. Technol. 133 (2015) 183–194, https://doi.org/10.1016/j.fuproc.2015.01.044.
[26] S. Chytil, A. Lind, E. Vanhaecke, E.A. Blekkan, Preparation and characterization of Mn_xO_y-Al_2O_3 sorbents for H_2S removal from biomass gasification gas, Energy Procedia 26 (2012) 98–106, https://doi.org/10.1016/J.EGYPRO.2012.06.015.
[27] J. Broekhoff, Studies on pore systems in catalysts IX. Calculation of pore distributions from the adsorption branch of nitrogen sorption isotherms in the case of open cylindrical pores A. Fundamental equations, J. Catal. 9 (1967) 8–14, https://doi.org/10.1016/0021-9517(67)90174-1.
[28] U. Holzwarth, N. Gibson, The Scherrer equation versus the "Debye-Scherrer equation, Nat. Nanotechnol. 6 (2011), https://doi.org/10.1038/nnano.2011.145, 534–534.
[29] M. Husmann, C. Hochenauer, X. Meng, W. De Jong, T. Kienberger, Evaluation of sorbents for high temperature in situ desulfurization of biomass-derived syngas, Energy Fuels 28 (4) (2014) 2523–2534, https://doi.org/10.1021/ef402254x.
[30] C. Julien, M. Massot, C. Poinsignon, Lattice vibrations of manganese oxides, Spectrochim. Acta Part A Mol. Biomol. Spectrosc. 60 (2004) 689–700, https://doi.org/10.1016/S1386-1425(03)00279-8.
[31] W. Li, X. Cui, R. Zeng, G. Du, Z. Sun, R. Zheng, S.P. Ringer, S.X. Dou, Performance modulation of α-MnO2 nanowires by crystal facet engineering, Sci. Rep. 5 (2015) 8987, https://doi.org/10.1038/srep08987.
[32] M. Baldi, F. Milella, J.M. Gallardo-Amores, G. Busca, A study of Mn-Ti oxide powders and their behaviour in propane oxidation catalysis, J. Mater. Chem. 8 (1998) 2525–2531, https://doi.org/10.1039/a803994a.
[33] S. Velu, N. Shah, T.M. Jyothi, S. Sivasanker, Effect of manganese substitution on the physicochemical properties and catalytic toluene oxidation activities of Mg–Al layered double hydroxides, Microporous Mesoporous Mater. 33 (1999) 61–75, https://doi.org/10.1016/S1387-1811(99)00123-7.
[34] M.B. Sreedhara, H.S.S.R. Matte, A. Govindaraj, C.N.R. Rao, Synthesis, characterization, and properties of few-layer MoO_3, Chem. Asian J. 8 (2013) 2430–2435, https://doi.org/10.1002/asia.201300470.
[35] D.P. Dutta, A. Mathur, J. Ramkumar, A.K. Tyagi, Sorption of dyes and Cu(II) ions from wastewater by sonochemically synthesized MnWO4 and MnMoO4 nanostructures, RSC Adv. 4 (2014) 37027–37035, https://doi.org/10.1039/c4ra07618d.